New Mexico Geological Society

Downloaded from: https://nmgs.nmt.edu/publications/guidebooks/41



Late Cenozoic rift tectonics and mountain-front landforms of the Sangre de Cristo Mountains near Taos, northern New Mexico

Christopher M. Menges

1990, pp. 113-122. https://doi.org/10.56577/FFC-41.113

in:

Tectonic Development of the Southern Sangre de Cristo Mountains, New Mexico, Bauer, P. W.; Lucas, S. G.; Mawer, C. K.; McIntosh, W. C.; [eds.], New Mexico Geological Society 41st Annual Fall Field Conference Guidebook, 450 p. https://doi.org/10.56577/FFC-41

This is one of many related papers that were included in the 1990 NMGS Fall Field Conference Guidebook.

Annual NMGS Fall Field Conference Guidebooks

Every fall since 1950, the New Mexico Geological Society (NMGS) has held an annual Fall Field Conference that explores some region of New Mexico (or surrounding states). Always well attended, these conferences provide a guidebook to participants. Besides detailed road logs, the guidebooks contain many well written, edited, and peer-reviewed geoscience papers. These books have set the national standard for geologic guidebooks and are an essential geologic reference for anyone working in or around New Mexico.

Free Downloads

NMGS has decided to make peer-reviewed papers from our Fall Field Conference guidebooks available for free download. This is in keeping with our mission of promoting interest, research, and cooperation regarding geology in New Mexico. However, guidebook sales represent a significant proportion of our operating budget. Therefore, only *research papers* are available for download. *Road logs*, *mini-papers*, and other selected content are available only in print for recent guidebooks.

Copyright Information

Publications of the New Mexico Geological Society, printed and electronic, are protected by the copyright laws of the United States. No material from the NMGS website, or printed and electronic publications, may be reprinted or redistributed without NMGS permission. Contact us for permission to reprint portions of any of our publications.

One printed copy of any materials from the NMGS website or our print and electronic publications may be made for individual use without our permission. Teachers and students may make unlimited copies for educational use. Any other use of these materials requires explicit permission.

This page is intentionally left blank to maintain order of facing pages.

LATE CENOZOIC RIFT TECTONICS AND MOUNTAIN-FRONT LANDFORMS OF THE SANGRE DE CRISTO MOUNTAINS NEAR TAOS, NORTHERN NEW MEXICO

CHRISTOPHER M. MENGES
U.S. Geological Survey–Al Ain Mission, National Drilling Company, Al Ain, United Arab Emirates

Abstract—Patterns and rates of faulting along the eastern margin of the Rio Grande rift in northern New Mexico are derived from geomorphic analysis of fault scarps, triangular facets, spur ridge crests, range crests and drainage basins on the Sangre de Cristo mountain front. Systematic variations in width, complexity and position of fault scarps and facets at the mountain-front base define a geometric fault segmentation pattern consisting of four primary segments 15 to 20 km in length, each with two to four, 5- to 10-km-long subsegments. Morphologic analysis of alluvial fault scarps suggests several late Holocene to latest Pleistocene surface ruptures that were complexly distributed among the segments and subsegments. Statistical analyses of map and field data on triangular facets indicate that variations in the geometry and/or rates of range-front faulting influence facet-slope gradient, height and slope area more than bedrock lithology of piedmont dissection. The steepest, highest, largest and least dissected basal facets occur above structurally simple, narrow zones in the central and southern parts of fault segments or subsegments. These sites commonly contain the youngest fault scarps, as well as the steepest, most convex, and least benched systems of faceted spurs on the range front. These patterns suggest a long-term persistence of fault segmentation through at least the Quaternary, further supported by lateral variations in the altitude of a prominent set of mid-escarpment benches. The amounts and rates of post-mid-Pliocene vertical displacements estimated from the bench heights vary systematically from 500 m (115 m/my) to 1124 m (261 m/my) with position along the range-bounding fault. The benches also define an abrupt change in the form and steepness of facet-spur ridge crests on the mountain front. They correspond in altitude to prominent knickpoints in the channel profiles of adjacent mountain-front drainage basins, and project into the top of distinct inner gorges in most canyons draining the interior of the Sangre de Cristo Mountains. The mid-Pliocene benches and related features appear to mark a major tectonic transition along this part of the rift, recorded in erosional landforms of the bordering range block.

INTRODUCTION

A number of geologic studies in the northern Rio Grande rift have described complex Cenozoic tectonism with several distinct evolutionary stages of mid-Miocene through Quaternary ages (Baltz, 1978; Hawley, 1978; Chapin, 1979; Machette and Colman, 1983; Baldridge et al., 1984; Morgan et al., 1986; Chapin et al., 1987). Many of these interpretations are based primarily on tectonic analyses of sedimentary and volcanic stratigraphy exposed in or adjacent to dissected rift basins. Miocene and (or) Pliocene rift tectonism is particularly difficult to decipher in undissected basins such as the Taos Plateau and the San Luis Valley where appropriately aged stratigraphic units are buried or only sparsely exposed along basin margins (e.g., McCalpin, 1982; Dungan et al., 1984; Manley, 1984; Rogers, 1984). The geomorphic effects of this tectonism, however, may be partially recorded in the morphology of erosional landforms in the escarpments and uplifted range blocks bordering rift basins. In many cases tectonic geomorphic analysis can be used to extract some of this tectonic information from rift-bounding landscapes (Bull, 1984, 1987; Mayer, 1986).

This paper summarizes a detailed study of the tectonic geomorphology of a 50-km-long section of the western mountain front of the Sangre de Cristo Mountains north of Taos in northern New Mexico (Fig. 1; Menges, 1988b). This study examined a variety of types and scales of mountain-front landforms, including fault scarps, triangular facets, spur ridge crests, range crests and drainage basins. The specific mountain-front landforms discussed in this paper are schematically illustrated in Figure 2 and defined as follows: (1) fault scarps—topographic scarps or steps that are the eroded remnants of vertical surface displacements on the fault trace, generally developed in piedmont alluvium of alluvial-mantled bedrock benches; (2) basal facets—triangular to polygonal-shaped bedrock hillslopes that represent the smallest undissected remnants of fault-line scarps at the base of the range front; (3) spurs—ridge crests extending upslope from the upper apices of basal triangular facets; (4) composite facets—triangular-shaped networks of basal facets, spurs and drainage basins that collectively represent the eroded remnants of large dissected facets; and (5) range crest—the highest ridgeline or upland forming the topographic boundary between the mountain front and the interior of the range block. Drainage basins developed by dissection of the range front are examined to a lesser extent.

The morphology of these mountain-front features were defined by: (1) field data, including topographic profiles and geomorphic-soil data measured on fault scarps and basal facets at 8 field sites (Fig. 3); (2) extensive measurements of size and slope-gradient characteristics of facets from USGS topographic maps with 40-foot (12.2 m) contour intervals; (3) construction from these maps of topographic profiles that follow the ridge crests of facet-spur systems on the range front; and

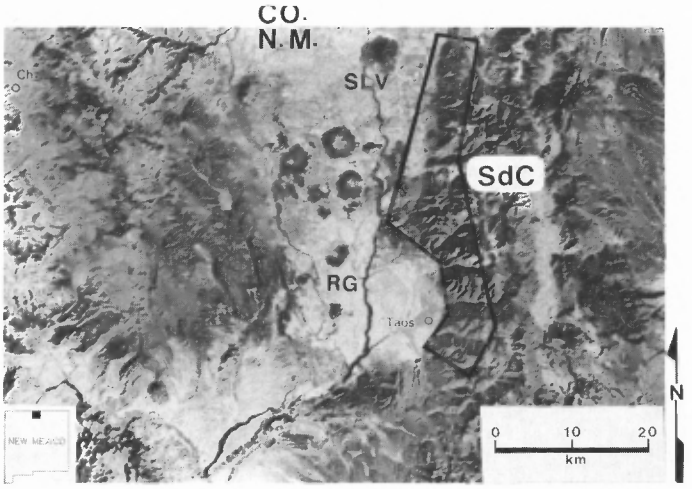


FIGURE 1. Location of study areas in the southern Sangre de Cristo Mountains near Taos. Large box in center outlines the part of the range-bounding fault zone and adjoining mountain front included in this study. Abbreviations are: Rio Grande gorge (RG); Sangre de Cristo Mountains (SdC); and southern San Luis Valley (SLV). Northern limit of map coincides with the Colorado (CO) and New Mexico (NM) border. (Adapted from composite Landsat image, New Mexico Geological Society, 1982.)

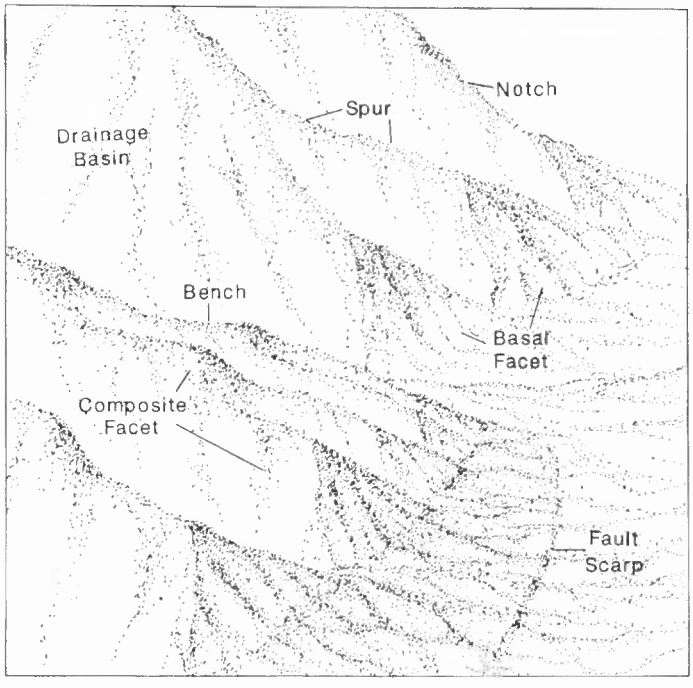


FIGURE 2. Sketch illustrating key erosional landforms of Sangre de Cristo mountain front analyzed in study. See text for landform definitions. Diagram modeled after section of mountain front above segment 1c, looking south (see Fig. 4). Drawn by Claire Reneau.

(4) systematic projection and plotting of the altitudes of the basal junction, range crest and selected erosional benches on the mountain front in a common vertical reference plane. These data were analyzed with a variety of numerical and statistical techniques such as linear and curvilinear regressions, time series analyses and parametric and nonparametric analysis of variance. This paper does not attempt to present detailed descriptions of these data and analyses (for detailed descriptions see Menges, 1987b, c, 1988a, b, in press). The following discussion focuses on the main results and conclusions of this study that provide information on short- and long-term patterns of tectonic activity on this part of the rift-bounding fault zone. These results are used to estimate the time-space resolution of tectonic interpretations that can be derived from appropriate geomorphic analyses of the differing scales of mountain-front landforms examined in the study.

STUDY AREA

The study area is a 50-km-long section of the bedrock mountain front of the southern Sangre de Cristo Mountains between Taos and the New Mexico–Colorado border (Figs. 1, 3). This prominent topographic escarpment trends north-south and slopes westward with 500 to 1200 m of local relief. In the Taos area, the highest summits of the mountain range reach altitudes of 3700 m; the adjacent basalt flows, basin fill, and piedmont alluvial fans of the southeastern San Luis basin lie at 2000- to 2700-m altitudes (Upson, 1939; Lambert, 1966). The range front contains a distinct suite of landforms (described above) that are characteristic of many tectonically active mountain fronts in the Basin and Range province (Wallace, 1978; Mayer, 1986).

The base of the main bedrock escarpment is structurally defined by a complex, normal-fault zone that dips at steep to moderate angles ($\geq 50°$) to the west. The fault zone forms the main eastern boundary of a narrow (5–15 km wide) graben in the adjacent part of the southeastern San Luis basin. This graben has an estimated depth of 2500 to 3000 m to the base of Tertiary fill (Keller et al., 1984). Together, the Sangre de Cristo fault zone and adjoining mountain front comprise the primary tectonic and physiographic boundary along the eastern margin of this part of the Rio Grande rift. A discontinuous series of middle(?) Pleis-

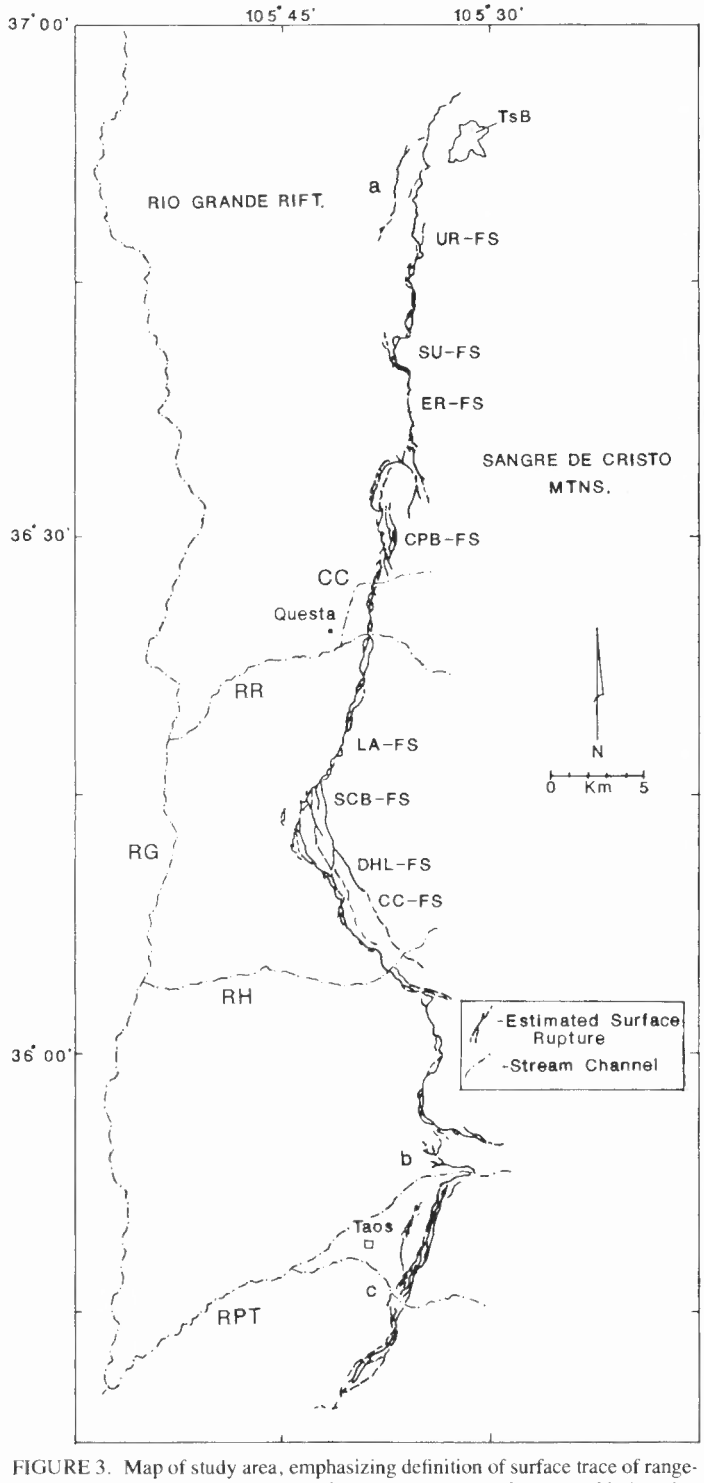


FIGURE 3. Map of study area, emphasizing definition of surface trace of range-bounding fault zone, as defined by fault scarps, the basal topographic junction of the mountain front and selected bedrock faults considered to be part of the boundary fault zone. Mapping based on interpretation of aerial photographs and detailed field work at eight sites (labeled in capital letters, that is, UR-FS). Three sites identified as a, b and c are from Machette and Personius (1984). Abbreviations for rivers: Rio Grande gorge (RG), Red River (RR), Cabresto Creek (CC) and Rio Hondo (RH). TsB is an outcrop of Pliocene basalt (Servilleta Basalts of Lipman et al., 1986) preserved at San Pedro Mesa on the north end of the range front.

tocene to Holocene fault scarps and faulted bedrock benches are developed along most sections of this fault zone (Fig. 3; Machette and Personius, 1984; Menges, 1987a, c, 1988b, in press).

The bedrock exposed in the range block within the study area include Precambrian (Proterozoic X) granitic rocks and mafic gneisses and schists overlain and intruded by mid- to upper-Tertiary volcanic and plutonic rocks (Reed et al., 1983; Reed, 1984). Paleozoic sedimentary rocks occur in the southernmost part of the mountain front near Taos. Most of the volcanic rocks are related to the formation of the Questa caldera and Latir volcanic field in late Oligocene time (Lipman et al., 1986). The mid-Tertiary volcanic rocks are displaced by an extensive network of low-angle normal faults that represent a mid- to late-Tertiary interval of rift extension that pre-dates formation of the present range block and basin (Lipman, 1981; Lipman and Reed, 1984).

Pliocene rifting was accompanied by extrusion of volcanic rocks of the Taos Plateau volcanic field, which contains widespread tholeiitic basalt flows and interstratified dacitic and andesitic vents with 2–5 Ma K-Ar dates (Lipman and Mehnert, 1979; Dungan et al., 1984; Lipman et al., 1986). The basalt flows are exposed extensively in the Rio Grande gorge and mantle the floor of the southern San Luis Valley in and adjacent to the study area. Within the study area, water-well logs and (or) exposures in the canyon walls of incised tributaries indicate that the basalt flows of the gorge extend eastward at shallow depths beneath the eastern San Luis Valley to near the base of the Sangre de Cristo mountain front (Winograd, 1959, 1985; Dungan et al., 1984; Summers and Hargis, 1984). Similar basalt flows with 4.3-Ma K-Ar ages also are preserved locally on top of San Pedro Mesa at the north end of the range block near the Colorado–New Mexico border (Fig. 3; Lipman et al., 1986). Thus, the difference in altitude between the basalt flows on the range block and those in the adjoining basin provides an approximate measure of the cumulative vertical offset along the range-bounding fault zone since 4.3 Ma (Lipman and Reed, 1984).

GEOMETRIC SEGMENTATION OF THE RANGE-FRONT FAULT

Segmentation patterns on the range-bounding fault zone originally were defined strictly on the basis of systematic variations in the geometry of its surface trace. The fault trace was determined by field and photointerpretive mapping of fault scarps and the topographic base of range-front facets (Fig. 3). These data suggest two complementary and generally overlapping scales of geometric fault segmentation, which consist of four primary segments, each 15–20 km in length and composed of two to four subsegments with 5–10 km lengths (Fig. 4a). Segments and subsegments are delineated by systematic spatial variations in the complexity and position of the surface trace of the fault zone relative to the range front (Figs. 4a, b). The central to south-central sections of most segments are characterized by confined fault zones (type A) localized at the base of mountain-front facets. More complex fault geometries (type B) typically occur near the termini, or boundaries, of segments and subsegments, where fault displacements are distributed over a broad zone of piedmont scarps and bedrock fault splays that bound progressively uplifted structural blocks. These variations in fault geometry also are accompanied by other changes in the relative position and elevation of the base of the range front itself (Fig. 5); structural segmentation of the range-front fault defines alternating series of high-elevation reentrants at the middle of segments and low-elevation salients at segment boundaries. The geometric and physiographic patterns that characterize segments and subsegments are similar in many ways. They differ from one another primarily in the scale and degree of development of the geometric variation described above. Most of the large segments also are associated with major changes in the altitudes, relative position, and (or) orientation of the overall mountain front. Segmentation patterns on the range-front fault are most pronounced at a relatively few transition zones between primary fault segments (e.g., the boundaries between segments 1–2 and 2–3; Fig. 4). These major boundaries are marked in planview by large right-stepping jumps in the base of the range front across a zone of overlap between the ends of adjoining segments.

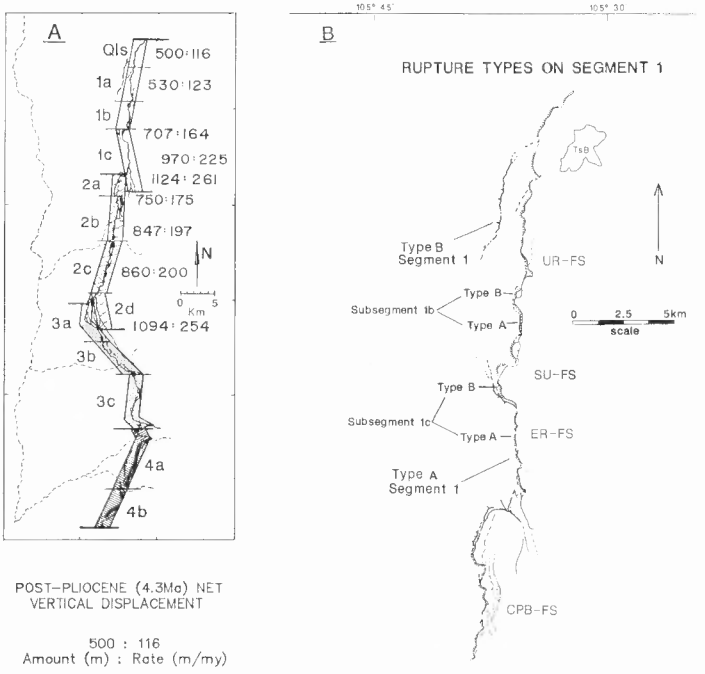


FIGURE 4. Geometric segmentation and post-Pliocene displacement patterns of range-bounding fault zone, interpreted from selected geomorphic and structural features along the mountain front. a, Map of geometric segmentation patterns in the surface trace of the range-bounding fault zone based on variations in the features presented in Figure 3 (defined in text). Four primary segments are bounded by the heavy lines and are indicated by numbers 1–4; subsegments are outlined by fine lines and are labeled with combination of lower-case letters and numbers. Other numbers to right of fault indicate amounts and average slip rates for post-Pliocene net vertical displacements at specific sites, estimated from heights of mid-escarpment benches that correlate with 4.3 Ma basalt flow (TsB, Fig. 3) on north end of range front (see text). b, Enlargment of fault segment 1 and northern part of segment 2 from Figures 3 and 4a, showing several examples of type A and type B rupture patterns (described in text) that are used to define geometric fault segmentation. Both types of ruptures are illustrated at segment and subsegment scales.

TIME-SPACE RUPTURE PATTERNS ON LATE QUATERNARY FAULT SCARPS

The relative timing of late Quaternary surface ruptures among fault segments and subsegments is estimated from morphologic and stratigraphic analyses of 40 alluvial fault scarps that were profiled in the field (Menges, 1987b, 1988b, in press). Cumulative vertical displacements of 4.5–10 m are estimated by application of the graphical techniques of Machette and Personius (1984) to topographic profiles of large multiple-rupture scarps developed in middle to late Quaternary surfaces; these composite scarps are interpreted to represent 2 to 5(?) individual rupture events, based on comparisons with 0.5–2.7 m offsets of latest Pleistocene to Holocene surfaces on nearby single-event scarps.

Age estimates of the most recent surface rupture(s) at various sites on the range-front fault are based on (1) linear regression analyses of maximum-slope-angle–log-height data from single-event and composite scarps (Bucknam and Anderson, 1979; Machette and Personius, 1984), and (2) diffusion modeling of 20 single-event scarps, using the technique of Nash (1980, 1984, 1987). The diffusion modeling technique used in the study estimates the formation (rupture) ages of fault scarps from a finite difference solution to a time-dependent diffusion equation that approximates the processes and rate of scarp degradation. Scarp age solutions are very sensitive to assumptions of initial scarp morphology and the degradation-rate constant used in modeling. These analytical uncertainties were incorporated statistically in this study by a modal histogram technique adapted from Mayer (1984) that provides modal and median ages for scarps estimated from a range of possible initial

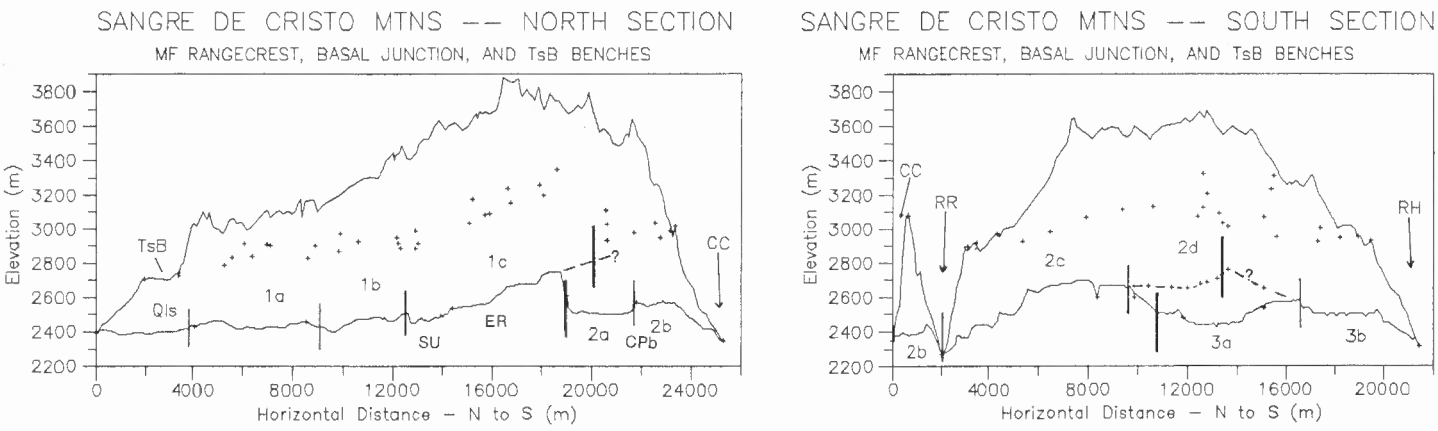


FIGURE 5. Plot of elevation of range crest, base and selected benches of the mountain front of the western Sangre de Cristo Mountains, subdivided into sections north and south of Cabresto Creek (CC). Altitudes from 1:100,000 and 1:24,000 scale maps are projected approximately perpendicular to the mountain front into a common vertical plane (5.4 × vertical exaggeration) oriented parallel to range front (see appendix D, Menges, 1988b, for detailed description of plotting procedures). Crosses indicate the projected positions of a set of prominent topographic benches at mid-escarpment levels on most facet-spur systems that correlate with Pliocene basalt flows (TsB; Fig. 3) at the north end of the range crest (see text for details; also Fig. 12). Alphanumeric labels refer to segments and subsegments of Figure 4a, with heavy and fine vertical lines indicating approximate segment and subsegment boundaries, respectively. Dashed horizontal lines indicate projected altitudes of the base of interior mountain fronts, i.e., large escarpments above subhorizontal bedrock benches within the main bedrock mountain front. Qls: areas of Quaternary landslides, derived from basalt flows (TsB), that bury range-front fault. Other symbols are river abbreviations of Figure 3. Projections of elevation surfaces on northern (Latir) section of range front (above). Projections of elevation surfaces on southern (San Cristobal) section of the mountain front (below).

morphologies and published rate constants (Fig. 6; Menges, 1988b, in press).

These morphologic scarp analyses, and particularly the diffusion modeling, suggest the following ages for the youngest rupture at various sites on the mountain front (Figs. 6, 7):

1. There is ample evidence for latest Pleistocene to Holocene surface rupture along most of the 50-km-long section of the range-front in the study area, with relatively younger rupture ages indicated for the northern part of the mountain front.

2. Variations in the morphology of scarps suggest a minimum of three discrete groups of rupture ages on various fault segments and subsegments which are consistent with offset relationships in Quaternary surfaces. These age categories are: (a) latest Pleistocene, evident only on piedmont fault scarps at some segment boundaries; (b) early to middle Holocene, related to one, or perhaps several, temporally clustered rupture(s) distributed along most of the range front in the study area; and (c) middle to late Holocene, restricted to one small subsegment (1c) 6 to 10 km in length at the south end of segment 1 (Figs. 4a, 7).

These data may be interpreted to represent three different, temporally distinct patterns of rupture segmentation. One large-scale rupture, or series of ruptures closely spaced in time, with average vertical displacements of 1.2 m, appears to have extended across several segment and subsegment boundaries along all or most of a 30–50-km length of the range-front during the early to middle Holocene. This type of event(s) may represent the dominant scale of surface rupture along most of the range-bounding fault. One short, discrete rupture with a relatively small vertical displacement of 0.8 m occurred on a single subsegment (1c, Figs. 4a, 7). There may be slightly greater offset of late Pleistocene surfaces at this locality as well. This type of small-scale rupture either filled in a gap in earlier Holocene rupture or, more likely, was superimposed across slightly older and larger multiple-segment events. There is a noticeable absence of Holocene rupture on piedmont scarps at the northern extremities of three major segments (Figs. 4a, 7). These apparent gaps in the Holocene event(s) probably represent zones of less frequent rupture and (or) small net displacements across these segment boundaries on the range-bounding fault zone.

INFLUENCE OF RANGE-FRONT FAULTING ON TRIANGULAR FACETS

Detailed analysis of map and field data on basal triangular facets provides information on the geomorphic framework of facet hillslopes and the relationships between facet morphology and tectonic activity on the range-front fault (see Menges, 1987b, 1988b). Field data were obtained from 40 transects that were measured upslope on undissected facets and keyed to observations on hillslope geomorphology, bedrock outcrop, and soil and colluvial stratigraphy. The average slope gradient, local height and slope area of all basal facets on the range front were also measured by interpreting data from 7.5′ USGS topographic quadrangle maps. Analyses of variance were applied to the latter data, in order to estimate the relative influence of fault segmentation patterns (using site position on the range-bounding fault as a proxy), bedrock lithology and the amount of piedmont dissection on facet morphology (Fig. 8). These results were then interpreted in the context of the field

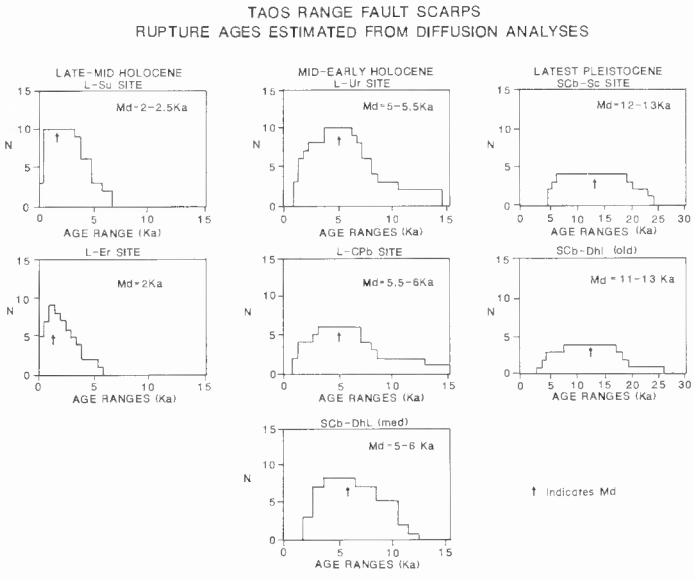


FIGURE 6. Modal-age histograms for single-rupture fault scarps profiled at 7 of the 8 field sites on the range-bounding fault zone (Fig. 3). Histograms are constructed from composite range of age estimates derived from diffusion modeling of all single-event scarps at a given site, using several initial morphologies and three possible diffusivity rate constants for each scarp (discussed in text; see also appendix C, Menges, 1988b, in press). Site histograms are arranged in 3 columns according to similarities in the median ages (Md) and general form of histogram. Mann-Whitney nonparametric tests indicate that the resulting 3 age categories are distinct from one another at $\alpha = 95\%$.

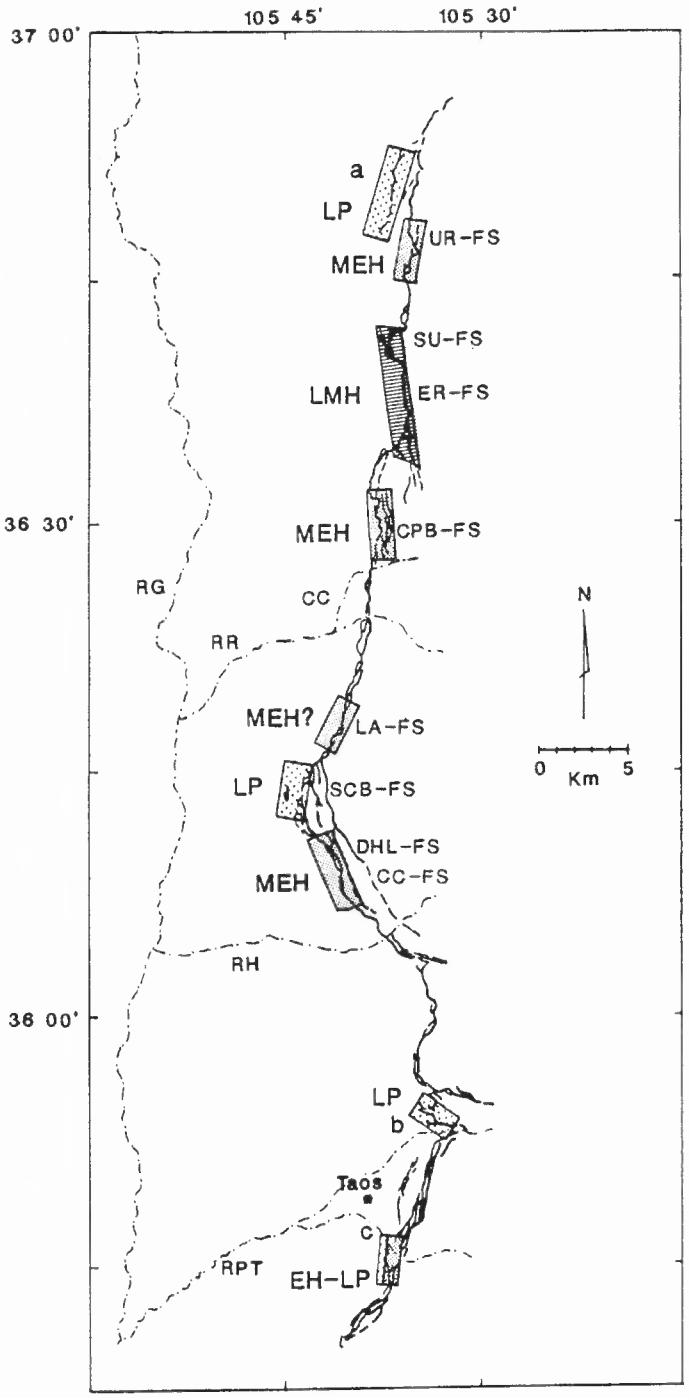


FIGURE 7. Distribution map of estimated ages for the most recent single-event fault scarps along the range-bounding fault zone. Data for estimates include: (1) combined diffusion modeling (see Fig. 6) and regression analyses at sites identified by capital letters (for example, UR-FS; see Fig. 3); and (2) regression analyses of piedmont fault scarps at sites a, b and c (see Fig. 3) from Machette and Personius (1984). Morphologic age estimates are consistent with stratigraphic constraints on the age of most recent rupture derived from offset geomorphic surfaces. General age categories for sections of the fault zone with patterned strips are: LP—latest Pleistocene, MEH—early to middle Holocene, LMH—middle to late Holocene, EHLP—latest Pleistocene to early Holocene.

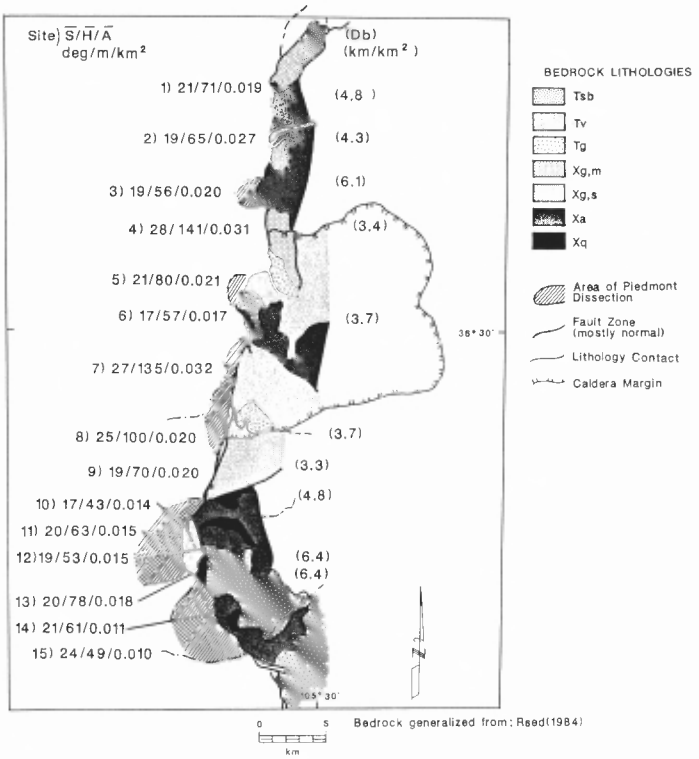


FIGURE 8. Map showing variations in selected morphologic variables of basal facets along mountain front, relative to fault segmentation patterns, bedrock lithology, and piedmont dissection. Site means of basal facet variables, measured at specific sites on USGS 7.5′ topographic maps, are listed to left of range front as follows: site number, S—average slope gradient, H—local height and A—slope area, corrected for average gradient. Average drainage density of 3rd-order drainage basins near or within facet sites are listed in parentheses, where available, to right of range front (from appendix I, Menges, 1988b). Left margin of mountain front approximately marks range-front fault of Figure 3. Major rock types indicated on map (from Reed, 1984, and Reed et al., 1983) are: TsB—Pliocene basalt flows (4.3 Ma radiometric age date); Tv—Tertiary volcanic rocks; Tg—Tertiary granitic plutons, Xg, m—Proterozoic-X granitic gneiss, Xg, s—Proterozoic-X granitic gneisses and schists; Xa—Proterozoic-X amphibolitic gneisses and schists; and Xq—Proterozoic-X quartzites. Also identified are areas of local and regional piedmont dissection and margin of late Oligocene caldera (Lipman et al., 1986).

data to develop a general geomorphic model interrelating these three external controls to facet form and evolution.

Morphology of basal facets

The morphometry of many basal facets at different sites on the mountain front falls within a relatively narrow range of slope gradients (19°–20°), heights (60–80 m) and slope areas (0.018–0.020 km^2) (Fig. 8). These morphologic characteristics probably reflect the dominant long-term tectonic, geomorphic, bedrock and climatic conditions operating on facet hillslopes along most of this range front.

Profile comparisons and statistical analyses suggest that segmentation-related variations in basal faulting are a major, and in many places dominant, influence on facets with morphologic parameters markedly different from the average values cited above (Fig. 8). The geometry (i.e., the confined vs. distributed patterns described above) and (or) relative rates of faulting affect major aspects of facet hillslopes such as average slope gradient, height, slope area and the degree and size of bench development at these sites. The majority of the inter-site facet variation is concentrated on parts of a few segments and subsegments. That is, sites on the central to south-central parts of these segments and subsegments with type A fault geometries contain unusually large, steep, undissected and unbenched facets; this contrasts with typically small, dissected, gently sloping, benched basal facets observed at nearby type B segmentation boundaries (Figs. 4b, 8, 9).

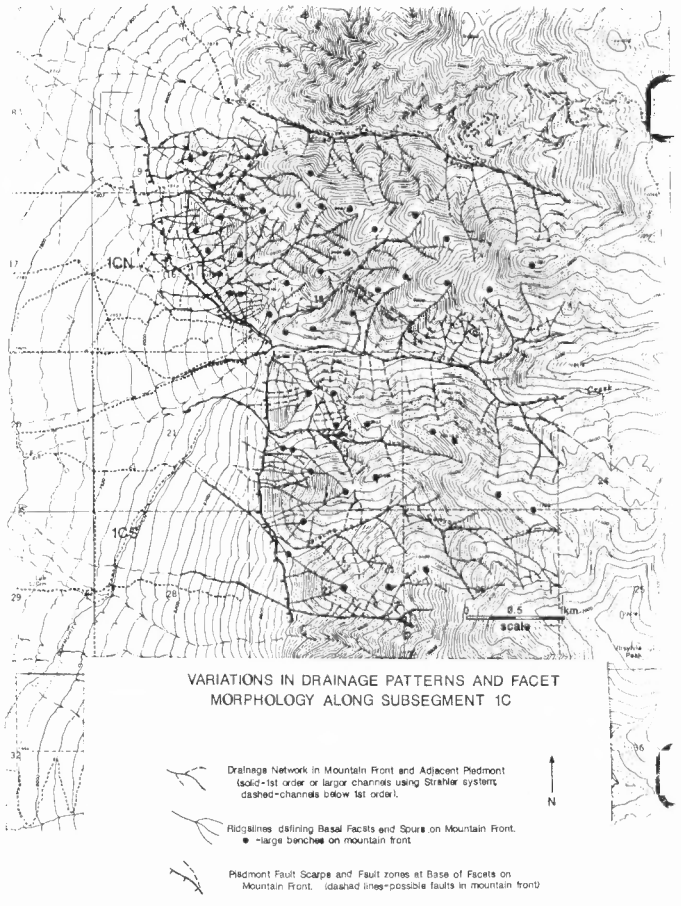


FIGURE 9. Map of variations in drainage patterns, facet morphology and rupture geometry along subsegment 1c. High-density drainage networks are developed on smaller benched facets above the complex multiple-rupture faulting at the northern termination of the subsegment (1cN). The large number of benches on these facets are produced by uplifted structural blocks and (or) intersections of the divides between adjacent drainages. The steep, high, unbenched facets above the single-strand fault in the middle of the subsegment (1cS) contain much lower density drainage networks.

Fault segmentation patterns also directly influence drainage patterns on facet hillslopes. The uplift and dissection of structural blocks between fault splays induce dense incised channel networks on benched facets above type B rupture on segment or subsegment boundaries (e.g., 1cN, Fig. 9). This contrasts with the relatively sparse and poorly integrated drainages observed on facet hillslopes above simple narrow type A fault patterns in the central or south-central parts of segments or subsegments (1cS, Fig. 9). The low-density channel development appears to favor accumulation of thick colluvial deposits with deep, well-developed soils on these high, steep facets (Menges, 1987b, 1988b).

Nontectonic variables such as bedrock lithology and piedmont dissection exert secondary, but locally significant, influences on facet morphology (Fig. 8). Bedrock lithology affects many of the detailed characteristics of facet hillslopes, including outcrop pattern and distribution, the characteristic size range of colluvial gravel, the type and extent of surface weathering and the amount of small-scale variation in slope angles on individual facet profiles. Most of these effects are related to a few rock types that are especially resistant or nonresistant to mechanical and physical weathering processes.

Piedmont dissection or aggradation primarily influences the density and degradation of stream channels that are developed on adjacent facet hillslopes, an effect enhanced by block uplift at fault segmentation boundaries, as was previously discussed. Dense, incised channel networks, in turn, produce small, low facets with numerous notches or small benches. Piedmont dissection does not appear to increase the gradient of most undissected portions of facets, except in uncommon situations where channels have downcut directly along the base of facets.

Long-term facet evolution

Profiles of facets with different heights at a given site on the range front commonly display marked similarities in general morphology and the type and amount of small-scale slope variation (Fig. 10). This facet hillslope form develops initially on low facet benches at heights of 15–30 m soon after bedrock is exposed near the crests of composite alluvial fault scarps. The resulting characteristic morphology appears to be maintained as the facet grows progressively in height and area with continued tectonic uplift at its base. These relations suggest that a given set of bedrock, piedmont, climatic and especially tectonic conditions on the range front produce a morphologic signature for undissected facet hillslopes, which is generally independent of scale.

LARGE-SCALE LANDFORMS OF THE MOUNTAIN-FRONT ESCARPMENT

Facet-spur systems and the mid-Pliocene topographic benches

Detailed topographic profiles of 15 facet-spur systems extending from the base of the mountain front to the range crest were measured from 7.5′ topographic quadrangle maps (Fig. 11). These profiles display variations in morphology that, like basal facets, correlate with position relative to geometric segmentation and fault-scarp rupture patterns on the range-bounding fault. The overall steepness and form of the large facet-spur profiles mimic morphologic patterns evident in the triangular facets at their base. This correspondence is striking especially in those characteristics such as relief, gradient and bench development which appear closely linked to segmentation patterns on the range-front fault zone. For example, the lower parts of facet-spur systems above the

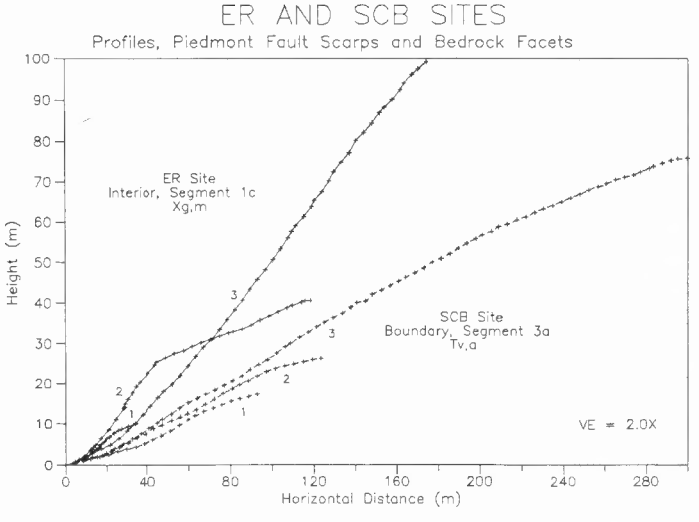


FIGURE 10. Two sets of transects illustrating morphologic evolution of fault scarps and basal facets in different tectonic, bedrock and piedmont environments on mountain front. Each set of transects is located at same site on range front with uniform fault patterns, bedrock and piedmont conditions, although the environmental settings differ between groups. The smallest transects in each group are composite (multiple-rupture) fault scarps in alluvium; the two larger transects are located on adjacent bedrock facets with different heights. The increasing heights of transects strictly reflects differential amounts of incremental faulting and uplift on the range-front fault. Each group therefore may be interpreted as a facet growth sequence, using a space-for-time substitution. The two bedrock facet transects in each group are remarkably similar in average steepness and degree of slope irregularity, reflecting characteristic morphologies for each tectonic-geomorphic setting that develop after bedrock is exposed on fault scarps. Labels for each set of profiles include: middle or boundary reaches of two fault segments (see Fig. 4a); and the following bedrock lithologies: Xg, m—Proterozoic-X granitic gneiss, and Tv, a—Tertiary andesites. The ER- and SCB-sites are located above an aggrading and dissected piedmont, respectively.

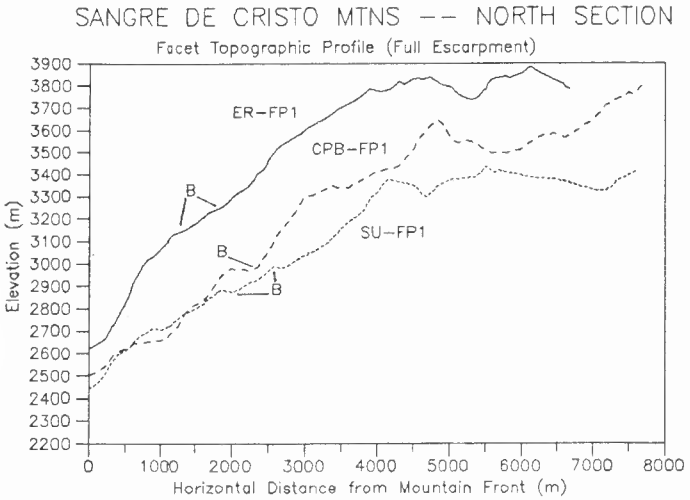


FIGURE 11. Three topographic profiles of the full mountain-front escarpment from 7.5-minute topographic maps. Profiles begin on piedmont below base of mountain front and extend upslope along facet-spur systems to range crest. Profiles begin at 3 sites used in fault-scarp and facet studies that are at the northern boundary and interior of subsegment 1c (SU-FS and ER-FS, respectively, Figs. 3, 4, 8) and at the northern end of subsegment 2a (CPB-FS). B marks the position of mid-escarpment benches correlated with the Pliocene basalts at the north end of the range crest (discussed in text; also Figs. 5, 12).

middle sections of many fault subsegments, when compared to the benched escarpment profiles at segmentation boundaries, are generally steeper, higher, more convex upwards and contain fewer wide benches (Fig. 11). Similar variations in the size and gradient of basal facets are observed at these sites as well (Figs. 8, 9).

The morphologic patterns described above generally extend upslope along facet-spur ridgelines to at least the altitude of a prominent set of mid-escarpment topographic benches (labeled B in Fig. 11). These benches are identified easily in every facet-spur system in the study area, and therefore they can be traced laterally along the range front to a broad geomorphic surface underlying the 4.3 Ma Pliocene basalts on San Pedro Mesa (Lipman et al., 1986) at the northern end of the range crest (Figs. 3, 5, 12). As noted earlier, these flows are correlated with extensive basalt flows that have similar 3–5 Ma radiometric age dates and that are widely distributed in the surface and shallow subsurface of the adjacent basin.

The mid-escarpment benches form a key mid-Pliocene reference surface on the range front that may be compared directly with fault segmentation patterns, fault scarp data and the morphology of lower facets and spurs. The highest-altitude Pliocene benches occur above fault subsegments near the south ends of segments with type A rupture patterns, the youngest fault scarps, the steepest and largest basal facets and the most convex facet-spur systems on the range front. This datum also can be used to directly estimate the net cumulative vertical displacements and average slip rates since 4.3 Ma (Figs. 4b, 5). For example, the southward variations of bench altitude above segment 1 imply a marked increase in post-basalt vertical displacements of 550 to 1124 m on the range-bounding fault zone, with 67% of this increase concentrated on subsegment 1c. A similar change in bench altitude is repeated southward along segment 2 as well. Conversely, the altitude of Pliocene benches and estimated fault displacements do not change appreciably across the boundaries of subsegments near the northern ends of segments that typically display less dramatic variation in small- to intermediate-scale tectonic landforms such as fault scarps and basal facets.

The morphology of most facet-spur profiles on the range front changes abruptly above the mid-escarpment Pliocene benches (Figs. 11, 12). The characteristic form and style of the lower range front generally do not continue on the upper part of spurs between the Pliocene bench and the range crest. The overall steepness of range-front spurs typically decreases on the upper escarpment, at least in part because of intense erosion and the antiquity of landforms at these altitudes. However, the mid-escarpment bench on many facet-spur profiles is a sharp inflection point marking a transition from a steep, convex lower part with few benches, to a more concave, highly benched and irregular upper section. Thus, the bench is interpreted to represent in part the morphologic imprint of a major change in the structural geometry and (or) rates of the range-bounding fault zone.

Associated landforms on the range front

A similarly sharp inflection point occurs in the longitudinal profile of stream channels in mountain-front drainage basins adjacent to facet-spur systems (Fig. 13). The master streams of almost all large drainage basins on the mountain front (3rd or 4th order, using the ordering system of Strahler, 1952; appendix 1, Menges, 1988b) display a prominent knickpoint somewhere in their upper reaches. The channel altitude at



FIGURE 12. Aerial view looking south of Pliocene basalt flows (in foreground) overlying a broad uplifted surface at the north end of the range crest (see Fig. 3). These flows are correlated southward with prominent topographic benches on facet-spur systems of the range front in distance (benches plotted in Figs. 5 and 11).

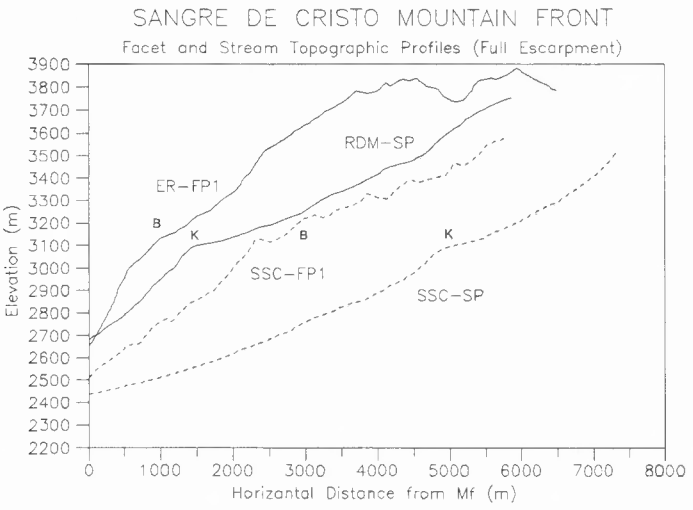


FIGURE 13. Two sets of superimposed topographic profiles of facet-spur systems (FP1) and longitudinal stream profiles (SP) measured on full mountain front escarpment from topographic maps. The facet and stream profiles of each pair are located adjacent to one another on the northern section (ER site above subsegment 1c—solid profiles) and on the southern section (SCB site above subsegments 3a–2d—dashed profiles) of the mountain front (cf., Figs. 3, 4a). B indicates level of Pliocene mid-escarpment bench on facet systems (Figs. 5, 12), and K denotes position of large composite knickpoint on stream profiles. Note the strong similarity in altitudes of benches and knickpoints developed on adjacent facets and stream channels, respectively.

the lip of the knickpoint matches quite closely the altitude of the mid-Pliocene bench on facet-spur divides to either side irrespective of underlying bedrock, position on the range front, or basin size (points labeled B and K, Fig. 13). However, the channel distance of knickpoints from the canyon mouths varies among drainage basins, depending on such factors as relative stream discharge and power, basin relief and catchment area and bedrock characteristics.

Topographic profiles across the valleys of large, 5th- or 6th-order streams draining the interior of the range block delineate a broad set of accordant slope breaks at midheight on the sideslopes of the canyons (e.g., Red River [RR], Cabresto Creek [CC] and Rio Hondo [RH]: Fig. 5). The paired benches on both sides of each canyon define a dissected platform that separates a steep, narrow inner gorge directly above the channel from the much wider and gently sloping sidewalls in the upper valley. This type of valley-in-valley profile indicates renewed or accelerated valley incision below the level of the mid-canyon benches. Canyon downcutting in this part of the Sangre de Cristo Mountains primarily reflects the intermixed base-level effects of local range-front faulting, regional dissection along the Rio Grande system, and fluvial responses to climatic changes in the Quaternary (Kelson, 1986; Wells et al., 1987).

The valley bench above the inner gorge in each canyon intersects the range front at approximately the same height as the mid-escarpment facet benches and the stream channel knickpoints described above (Figs. 5, 13). This relationship suggests that the range-front faulting responsible for uplift of the Pliocene bench is also an imporant factor in producing the valley-in-valley cross-profiles. There is a marked concordance among the relative altitudes of benches developed on many disparate hillslope and fluvial components of the mountain-front landscape. The benches and knickpoints collectively define a distinct topographic datum of probable early Pliocene age, which appears to record a major tectonic and physiographic transition in the late Cenozoic evolution of this rift-bounding range block.

Range-crest elevations

The projections of Figure 5 indicate a strong subparallelism in the heights of the range crest, the uplifted Pliocene benches, and the fault trace at the base of the mountain front. The highest altitudes on the range front (e.g., the Latir Peaks and San Cristobal areas, Figs. 5a and b, respectively) are positioned above the southern parts of fault segments 1 and 2, which are associated with the highest altitudes of the mid-escarpment benches and especially large, steep, triangular facets and facet-spur systems. The latter landforms are interpreted to represent relatively high levels of tectonic activity on these sections of the range-bounding fault. Some of the local increase in range-crest altitudes may reflect in part additional relief generated by the cumulative vertical displacements on the overlapping ends of adjoining fault segments at these sites on the basal fault zone. These patterns collectively suggest that some of the local variation in range-crest heights results from post-Pliocene segmentation patterns on the range-bounding fault zone. A significant component of local range-crest relief, however, is probably inherited from antecedent Tertiary tectonism and (or) volcanism in the range block (see tectonic section below).

NEOTECTONIC AND STRUCTURAL INTERPRETATIONS OF RANGE-FRONT FAULTING

Short-term patterns

Paleoseismicity

The fault-scarp data suggest that segmentation patterns on the range front may be associated with two scales of surface ruptures. The contrasting sizes in coseismic rupture imply at least two magnitudes in potential paleoearthquakes. Surface ruptures with offsets of less than 1 m confined to subsegments of 5–10 km in length would be associated with earthquakes of 5.8–6.3 magnitude, based on several methods of estimating paleoearthquake magnitudes from the amount and length of surface ruptures (Hanks and Kanamori, 1979; Slemmons, 1982; Machette, 1986, 1988). The same techniques indicate earthquakes of 6.8–7.1 magnitude if vertical displacements 1.2 m in size extend across contiguous groups of segments and subsegments with cumulative lengths of 30–50 km, as postulated earlier.

Recurrence intervals and late Quaternary slip rates

The fault-scarp analyses do not provide good estimates of recurrence rates, but the available data suggest general recurrence intervals on the order of 10^4 yrs between individual events at a given site on the range front (Menges, 1987a, c, in press). These estimates are compatible with 10–50 Ka recurrence determined for ruptures on the north end of the Sangre de Cristo fault zone in Colorado by McCalpin (1982).

Late Quaternary slip rates on the range-front fault zone also are difficult to estimate accurately with the available geochronologic control. The amount of offset on middle(?) to late Pleistocene surfaces suggests average displacement rates much less than 0.1 mm/yr, and probably on the order of 0.03–0.06 mm/yr.

Long-term patterns

Post-Pliocene persistence of fault segmentation

The morphology of different scales of mountain-front landforms correlates closely with those characteristics that appear to best reflect tectonic activity on the range-bounding fault zone. For example, subsegment 1c is associated with mid to late Holocene fault scarps, unusually steep, large and unbenched basal facets, steep, convex, facet-spur systems, the highest altitudes of the mid-escarpment bench, and the locally highest section of the range crest (Figs. 5, 7, 8, 11). These relationships indicate that many segmentation patterns evident in late Quaternary rupture, including some at subsegment scale, have persisted over the post-4 Ma interval of deformation recorded below the uplifted Pliocene bench.

Long-term slip rates

The estimated vertical offset of the Pliocene basalts and related bench suggest cumulative amounts and rates of post-Pliocene displacements of 500–1124 m and 115–261 m/my, respectively. These displacement estimates compare favorably with uplift rates of 210 m/my for the range block derived from fission track dating of mid-Tertiary plutons (Kelley and Duncan, 1984, 1986). The long-term slip rates on the range-front fault, however, are approximately two to eight times greater than equivalent-unit slip rates inferred from Pleistocene scarps on the range-bounding fault zone (i.e., 30–60 m/my; see above). The differences between slip estimates may result from sampling different parts or scales of a complex seismic cycle (Pierce, 1986), or they may indicate actual waning of tectonic activity on the range-front fault in the late Quaternary.

The long-term slip rates cited above are comparable with or somewhat higher than equivalent-unit slip rates estimated for the Rio Grande rift in central and southern New Mexico (e.g., 60–120 m/my; Machette and Personius, 1984; Machette, 1987a). The long-term rates in both parts of the Rio Grande rift are considerably higher than the estimated Quaternary slip rates on scattered faults in southwestern New Mexico and southeastern Arizona (5–20 m/my; Pearthree et al., 1983; Machette et al., 1986). Similar estimates of long-term slip are not readily available for the Great Basin, but estimates of the late Quaternary slip rate on the Wasatch fault (1–2 mm/yr in the Holocene and 0.1–0.3 mm/yr in late Pleistocene; Machette, 1987b) and on range-front faults in central Nevada (0.5–1 mm/y; Thompson and Burke, 1973; Pearthree and Demsey, 1978) generally are higher than the late Quaternary slip rates estimated for the Sangre de Cristo fault zone (see above; also McCalpin, 1982; Menges, 1988b, in press).

Tectonic episodicity

The contrasting morphologies of the mountain-front escarpment above and below the Pliocene bench suggest that the bench surface represents a major shift in rift deformation. The upper part of the range front probably reflects an erosional landscape inherited from an earlier interval of landscape evolution and (or) rift tectonism before or during

late Miocene time. At some point after 4 Ma, deformation began and (or) was renewed on the present range-front system. By that time the modern basin-and-range topography and structure had begun to form concomitant with basaltic volcanism of the Taos Plateau volcanic field (Dungan et al., 1984).

The mid-escarpment bench, if erosional in origin, indicates a possible lull in tectonic activity on or near this mountain front. The bench may be fault-bounded in some areas, however, in which case it might represent geometric reorganization of local deformation along this rift boundary. Regardless, the presence of the bench indicates that some important transitions in rift tectonism observed in basin fill or volcanic stratigraphy also may be recorded in the erosional landscapes of boundary escarpments and the adjoining range blocks.

CONCLUSIONS

The geomorphic analyses described above indicate that the morphology of erosional landforms of the Sangre de Cristo mountain front contains significant information on rift tectonism. The landforms analyzed in this study vary considerably in vertical and horizontal scales, ranging from alluvial fault scarps (10^0 to 10^1 m high) at the base of the mountain front, through triangular facets (10^1 to 10^{2+} m), to facet-spur and drainage basins of the full range-front escarpment (10^3 to 10^4 m). These scale changes are associated with differing time intervals of tectonic and geomorphic evolution recorded in the morphology of each type of landform as well (Fig. 14). For example, fault scarps are the direct surface expression of small individual displacements on the boundary fault that occurred within middle to late Quaternary time (10^2 to 10^5 yrs). The form of the lower parts of facet-spur networks reflects the more generalized cumulative effects of long-term uplift on the range-front at intervals between the Pliocene and (or) Quaternary (10^5 to 10^6 yrs). The onset of rift tectonism that produced the modern topography is apparently recorded in a distinct topographic discontinuity in facet-spur networks, longitudinal profiles of mountain-front drainages and cross-sectional profiles of major canyons in the range block. Thus, most of the range crest and the upper part of the mountain front above the Pliocene benches are the uplifted, highly eroded remnants of an earlier landscape that mainly developed during pre-Pliocene tectonic and volcanic events (i.e., 10^6 to 10^7 yrs), although some of the local variation in the height of the range crest correlates directly with segmentation patterns in the range-bounding fault zone.

These relationships are summarized in the dashed lines in Figure 14, which provide estimates of the time-space resolution (i.e., level of detail) of neotectonic information recorded in various scales of mountain-front landforms. This resolution is governed in part by the approximate balance between tectonic activity on mountain-front faults and the erosional modification of fault-generated hillslopes on the range front. In a sense, the time-space band enclosed by these lines delimits the potential range of tectonic or geomorphic interpretations that can be extracted by analyses of mountain-front landforms in the particular deformational, geologic and climatic environment of this part of the Rio Grande rift.

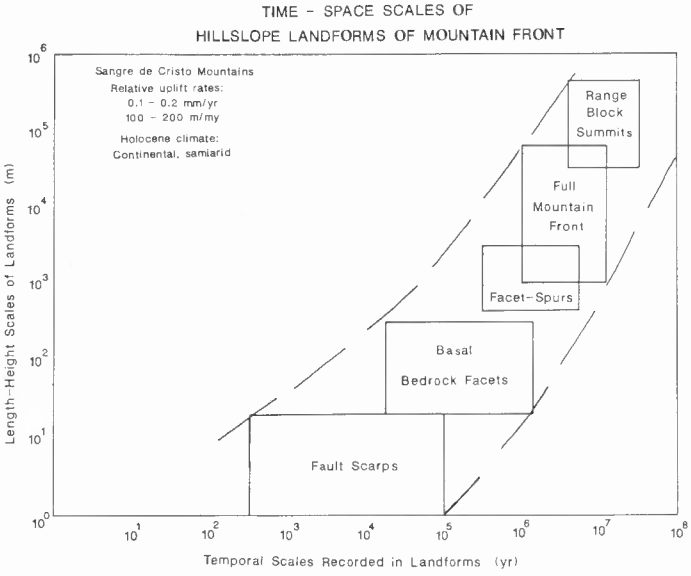


FIGURE 14. Diagram of inferred relationship between spatial (length-height) scales of mountain front landforms and general time intervals of tectonic or geomorphic processes potentially recorded in their morphology. Boxes indicate approximate boundaries of time-space scales for each landform type. The resolution, e.g., level of detail, of information decreases with increasing time-space scales as well. The estimated temporal limits of landforms are calibrated from several different geomorphic analyses discussed in text. Short- and long-term uplift rates derived from fault scarp and escarpment bench data (listed in upper left) furnish additional age guidelines for landforms of varying height on the lower range front. Heavy dashed lines delimit time-space resolution of different tectonic landforms on the mountain front. This indicates the approximate balance between relative rates of tectonic uplift on the range front and erosional modification of landforms. The resolution band is itself determined by the size of landforms vs. tectonic and environmental factors in the study area.

ACKNOWLEDGMENTS

This paper is a summary of dissertation research conducted at the University of New Mexico. I would like to acknowledge partial financial support for this research from the following funding sources: a Challenge Scholarship grant from the Office of Graduate Studies at the University of New Mexico, funds provided by the New Mexico Bureau of Mines and Mineral Resources, the 1986 New Mexico Geological Society Fellowship and a 1986 Mackin and general grant-in-aid from the Geological Society of America. I would like to thank my dissertation advisor, S. G. Wells, and other committee members (L. McFadden, J. Callender, J. Hawley and C. Mawer) for helpful comments and review of this part of my dissertation. This manuscript also has benefited from thoughtful reviews by J. C. Dohrenwend and M. Pavich. However, I assume ultimate responsibility for all analyses and interpretations in this article.

REFERENCES

Baldridge, W. S., Olsen, K. H. and Callender, J. F., 1984, Rio Grande rift: problems and perspectives: New Mexico Geological Society, Guidebook 35, pp. 1–12.

Baltz, E. H., 1978, Resume of Rio Grande depression in north-central New Mexico: New Mexico Bureau of Mines and Mineral Resources, Circular 163, pp. 210–228.

Bucknam, R. C. and Anderson, R. E., 1979, Estimation of fault-scarp ages from a scarp-height–slope-angle relationship: Geology, v. 7, pp. 11–14.

Bull, W. B., 1984, Tectonic geomorphology: Journal of Geological Education, v. 32, pp. 310–324.

Bull, W. B., 1987, Relative rates of long-term uplift of mountain fronts; *in* Crone, A. J. and Omdahl, E. M., eds., Proceedings of Conference XXXIX—Directions in Paleoseismology: U.S. Geological Survey, Open-file Report 87-673, pp. 192–202.

Chapin, C. E., 1979, Evolution of the Rio Grande rift—a summary; *in* Reicker, R. E., ed., Rio Grande rift: tectonics and magmatism: Washington, D.C., American Geophysical Union, pp. 1–5.

Chapin, C. E., Cather, S. M. and McIntosh, W., 1987, Evolution of the Rio Grande rift: an outline: Geological Society of America, Abstracts with Programs, v. 19, p. 617.

Dungan, M. A., Muehlberger, W. R., Leininger, L., Peterson, C., McMillan, N. J., Gunn, G., Lindstrom, M. and Haskin, L., 1984, Volcanic and sedimentary stratigraphy of the Rio Grande gorge and the late Cenozoic geologic evolution of the southern San Luis Valley: New Mexico Geological Society, Guidebook 35, pp. 157–170.

Hanks, T. C. and Kanamori, H., 1979, A moment magnitude scale: Journal of Geophysical Research, v. 84, pp. 2348–2350.

Hawley, J. W., ed., 1978, Guidebook to the Rio Grande rift in New Mexico and Colorado: New Mexico Bureau of Mines and Mineral Resources, Circular 163, 241 pp.

Keller, G. R., Cordell, L., Davis, G. H., Peeples, W. J. and White, G., 1984, A geophysical study of the San Luis basin: New Mexico Geological Society, Guidebook 35, pp. 51–57.

Kelley, S. A. and Duncan, I. J., 1984, Tectonic history of the northern Rio Grande rift derived from apatite fission-track geochronology: New Mexico Geological Society, Guidebook 35, pp. 67–73.

Kelley, S. A. and Duncan, I. J., 1986, Late Cretaceous to middle Tertiary tectonic history of the northern Rio Grande rift, New Mexico: Journal of Geophysical Research, v. 91, pp. 6246–6262.

Kelson, K. I., 1986, Long-term tributary adjustments to base-level lowering, northern Rio Grande rift, New Mexico [M.S. thesis]: Albuquerque, University of New Mexico, 211 pp.

Lambert, P. W., 1966, Notes on the late Cenozoic geology of the Taos-Questa area, New Mexico: New Mexico Geological Society, Guidebook 17, pp. 43–50.

Lipman, P. W., 1981, Volcano-tectonic setting of Tertiary ore deposits, southern Rocky Mountains: Arizona Geological Society Digest, v. 14, pp. 199–213.

Lipman, P. W. and Mehnert, H. H., 1979, The Taos Plateau volcanic field, northern Rio Grande rift, New Mexico; *in* Reicker, R. E., ed., Rio Grande rift: tectonics and magmatism: Washington, D.C., American Geophysical Union, pp. 289–311.

Lipman, P. W. and Reed, J. C., 1984, Second-day road log, from Taos to Hondo Canyon, Questa, Red River, Amalia, and back to Taos: New Mexico Geological Society, Guidebook 35, pp. 321–347.

Lipman, P. W., Mehnert, H. H. and Naeser, C. W., 1986, Evolution of the Latir volcanic field, northern New Mexico, and its relation to the Rio Grande rift, as indicated by potassium-argon and fission track dating; Journal of Geophysical Research, v. 91, pp. 6329–6345.

Machette, M. N., 1986, History of Quaternary offset and paleoseismicity along the La Jencia fault, central Rio Grande rift, New Mexico: Bulletin of the Seismological Society of America, v. 76, pp. 259–272.

Machette, M. N., 1987a, Neotectonics of the Rio Grande rift, New Mexico: Geological Society of America, Abstracts with Programs, v. 19, p. 754.

Machette, M. N., 1987b, Changes in long-term versus short-term slip rates in an extensional environment; *in* Crone, A. J. and Omdahl, E. M., eds., Proceedings of Conference XXXIX—Directions in Paleoseismology: U.S. Geological Survey, Open-file Report 87-673, pp. 228–238.

Machette, M. N., 1988, Quaternary movement along the La Jencia fault, central New Mexico: U.S. Geological Survey, Professional Paper 1440, 82 pp.

Machette, M. N. and Colman, S. J., 1983, Age and distribution of Quaternary faults in the Rio Grande rift—evidence from morphometric analysis of fault scarps: Geological Society of America, Abstracts with Programs, v. 15, p. 320.

Machette, M. N. and Personius, S. F., 1984, Map of Quaternary and Pliocene faults in the eastern part of the Aztec 1×2 quadrangle and the western part of the Raton 1×2 quadrangle, northern New Mexico: U.S. Geological Survey, Miscellaneous Field Studies Map MF-1465-B, scale 1:250,000, with text, 20 pp.

Machette, M. N., Personius, S. F., Menges, C. M. and Pearthree, P. A., 1986, Map showing Quaternary and Pliocene faults in the Silver City $1° \times 2°$ quadrangle and Douglas $1° \times 2°$ quadrangle, southeastern Arizona and southwestern New Mexico: U.S. Geological Survey, Miscellaneous Field Investigations Map MF-1465-C, scale 1:250,000, with text, 20 pp.

Manley, K., 1984, Brief summary of the Tertiary geologic history of the Rio Grande rift in northern New Mexico: New Mexico Geological Society, Guidebook 35, pp. 63–66.

Mayer, L., 1984, Dating Quaternary fault scarps formed in alluvium using morphologic parameters: Quaternary Research, v. 22, pp. 300–313.

Mayer, L., 1986, Tectonic geomorphology of escarpments and mountain fronts; *in* Active tectonics: studies in geophysics: Washington, D.C., National Research Council, National Academy Press, pp. 125–135.

McCalpin, J. P., 1982, Quaternary geology and neotectonics of the west flank of the northern Sangre de Cristo Mountains, south-central Colorado: Colorado School of Mines Quarterly, v. 77, 97 pp.

Menges, C. M., 1987a, Time-space segmentation of late-Quaternary rupture along the western Sangre de Cristo mountain front, north-central New Mexico: Geological Society of America, Abstracts with Programs, v. 19, p. 321.

Menges, C. M., 1987b, The form and evolution of bedrock facet hillslopes along the tectonically-active mountain front of the western Sangre de Cristo Mountains, northern New Mexico: Geological Society of America, Abstracts with Programs, v. 19, p. 770.

Menges, C. M., 1987c, Temporal and spatial segmentation of Pliocene-Quaternary fault rupture along the western Sangre de Cristo mountain front, New Mexico; *in* Crone, A. J. and Omdahl, E. M., eds., Proceedings of Conference XXXIX—Directions in Paleoseismology: U.S. Geological Survey, Open-file Report 87-673, pp. 203–222.

Menges, C. M., 1988a, Tectonic origin of facet benches on a normal-fault-bounded mountain front: an alternative model: Geological Society of America, Abstracts with Programs, v. 20, p. 215.

Menges, C. M., 1988b, The tectonic geomorphology of mountain-front landforms in the northern Rio Grande rift near Taos, New Mexico [Ph.D. dissertation]: Albuquerque, University of New Mexico, 339 pp.

Menges, C. M., in press, Late Cenozoic fault scarps, mountain-front landforms, and Pliocene-Quaternary segmentation of the range-bounding fault zone, Sangre de Cristo Mountains, New Mexico; *in* Krinitzsky, E. L. and Slemmons, D. B., eds., Neotectonics in Earthquake Evaluation: Reviews in Engineering, v. 8: Geological Society of America, Special Paper.

Morgan, P., Seager, W. R. and Golombek, M. P., 1986, Cenozoic thermal, mechanical and tectonic evolution of the Rio Grande rift: Journal of Geophysical Research, v. 91, pp. 6263–6276.

Nash, D. B., 1980, Morphologic dating of degraded normal fault scarps: Journal of Geology, v. 88, pp. 353–360.

Nash, D. B., 1984, Morphologic dating of fluvial terrace scarps and fault scarps near West Yellowstone, Montana: Geological Society of America Bulletin, v. 95, pp. 1413–1424.

Nash, D. B., 1987, SLOPEAGE program, v. 2.1: Fenneman-Rich Geomorphic Laboratories, Department of Geology, University of Cincinnati, Cincinnati, OH 45221-0013.

New Mexico Geological Society, 1982, New Mexico highway geologic map: New Mexico Geological Society, in cooperation with New Mexico Bureau of Mines and Mineral Resources, scale 1:1,000,000.

Pearthree, P. A. and Demsey, K., 1987, Patterns of Holocene faulting and the rate of extension in central Nevada: Geological Society of America, Abstracts with Programs, v. 19, p. 802.

Pearthree, P. A., Menges, C. M. and Mayer, L., 1983, Distribution, recurrence and possible tectonic significance of late Quaternary faulting in Arizona: Arizona Bureau of Geology and Mineral Technology, Open-file Report 83-23, 50 pp.

Pierce, K. L., 1986, Dating methods; *in* Active Tectonics, Studies in Geophysics: Washington, D.C., National Research Council, National Academy Press, pp. 195–214.

Reed, J. C., Jr., 1984, Proterozoic rocks of the Taos Range, Sangre de Cristo Mountains, New Mexico: New Mexico Geological Society, Guidebook 35, pp. 179–185.

Reed, J. C., Lipman, P. W. and Robertson, J. E., 1983, Geologic map of the Latir Peak and Wheeler Peak Wildernesses and Columbine-Hondo Wilderness Study Area, Taos County, New Mexico: U.S. Geological Survey, Miscellaneous Field Studies Map MF-1570-B, scale 1:50,000.

Rogers, K., 1984, A paleontological analysis of the Alamosa Formation (south-central Colorado: Pleistocene: Irvingtonian): New Mexico Geological Society, Guidebook 35, pp. 151–155.

Slemmons, D. B., 1982, Determination of design earthquake magnitudes for microzonation: Proceedings of the Third International Earthquake Microzonation Conference, v. 1, pp. 119–130.

Strahler, A. N., 1952, Dynamic basis of geomorphology: Geological Society of America Bulletin, v. 63, pp. 923–938.

Summers, W. K. and Hargis, L. L., 1984, Hydrologic cross section through Sunshine Valley, Taos County, New Mexico: New Mexico Geological Society, Guidebook 35, pp. 245–248.

Thompson, G. A. and Burke, D. B., 1973, Rates and direction of spreading in Dixie Valley, Basin and Range: Geological Society of America Bulletin, v. 84, pp. 627–632.

Upson, J. E., 1939, Physiographic subdivisions of the San Luis Valley, southern Colorado: Journal of Geology, v. 47, pp. 721–736.

Wallace, R. E., 1978, Geometry and rates of change of fault-generated range-fronts, north-central Nevada: Journal of Research, U.S. Geological Survey, v. 6, pp. 637–650.

Wells, S. G., Kelson, K. I. and Menges, C. M., 1987, Quaternary evolution of fluvial systems in the northern Rio Grande rift, New Mexico and Colorado: implications for entrenchment and integration of drainage systems; *in* Menges, C. M., Enzel, Y. and Harrison, B., eds., Friends of the Pleistocene–Rocky Mountain Cell, Fieldtrip Guidebook, pp. 55–69.

Winograd, I. J., 1959, Ground-water conditions and geology of Sunshine Valley and western Taos County, New Mexico: New Mexico State Engineer, Technical Report 12, 70 pp.

Winograd, I. J., 1985, Commentary on hydrologic cross-section through Sunshine Valley, Taos County, New Mexico, by W. K. Summers and L. L. Hargis: New Mexico Geology, v. 7, pp. 54–55.